Journal of Molecular Graphics and Modelling 72 (2017) 16–24

Contents lists available at ScienceDirect

Journal of Molecular Graphics and Modelling

journal homepage: www.elsevier.com/locate/JMGM

ISO-MANM: An imitation based optimization tool for multilayer microwave absorbers

A. Cheraghi[a,b], R. Malekfar[a,*], S. Moemen Bellah[c], M. Parishani[a]

[a] Department of Physics, Faculty of Basic Sciences, Tarbiat Modares University, Tehran P.O. Box 14115-175, I.R., Iran
[b] Faculty of Basic Sciences, Shahid Sattari University, Tehran, I.R., Iran
[c] Department of Process Modeling and Control, Faculty of Engineering, Iran Polymer and Petrochemical Institute, Tehran, I.R., Iran

ARTICLE INFO

Article history:
Received 8 October 2016
Received in revised form
24 November 2016
Accepted 25 November 2016
Available online 30 November 2016

Keywords:
Modeling
Layered structures
Nanocomposites
Polymers
Carbon nanotubes

ABSTRACT

We investigate the performance of 109 types of composition with complex permittivity and permeability properties in the frequency range of 1–12 GHz. The components of these compositions are based on conductive and nonconductive polymer composites, ferrites, hexaferrites, and carbon materials. A new swarm-based algorithm has been introduced to solve microwave absorbing nanomaterials (MANM) problem, called Imitation Based Optimization (ISO). The individuals in the ISO imitate each other and move to better locations. ISO has high ability to trade-off between the exploration and exploitation with setting the input parameters. Also, it can simultaneously deal with contentious and discrete spaces. The results show that our proposed method has high quality outcomes and can be used in various applications. Various outputs will be achieved by the presented tool for the aforementioned compositions as a general reference. Considering the ability of the presented tool for selecting layer priority, layer arrangement, layer thickness, frequency range, and incidence angles, a variety of analyses can be carried out. Another ability of the presented tool is analysis of the reflection loss at different incident angles in the microwave frequency range. Using the introduced tool, the reflection loss with TM and TE polarization analysis also can be calculated.

Introduction

Nowadays, in many high technology fields, the absorption of electromagnetic waves in microwave range is very important. Developing a wide variety of wireless electronic devices needs extensive knowledge of electromagnetic and material interaction, which provides an effective and low cost shielding for dealing with unwanted radiation. In aerospace science, development of the lightweight absorbing materials in a broad range of frequencies is an essential part of the electromagnetic wave absorption technology to minimize microwave reflection [1]. Nanomaterials are suitable choices as electromagnetic absorbers as they have unique mechanical and electrical properties. The composites based on nanoscale materials can be thin, lightweight, low cost, and easily manufactured especially for coating purposes [2].

Electromagnetic Interference (EMI) is a disturbance that affects an electrical circuit of a device due to an electromagnetic radiation from another electrical circuit [3]. Numerous personal electronic devices are in use today and protecting them from unwanted interaction waves in a broad range of electromagnetic frequencies is essential. Furthermore, moving to a lower scale in dimensions is necessary to obtain thin, lightweight, easy to manufacture, and low cost shielding materials.

Considering the fact that combination of different materials can have different magnetic and electrical losses and in practice we face electromagnetic absorbers with complex electrical and magnetic losses, various loss mechanisms for these combinations must be applied. For this reason, the cumulative absorption effects are taken into consideration. Materials selection combined with optimal structural design is required to describe MANM's performance in terms of its wave impedance, intrinsic impedance of layers, polarization of the incident waves, incident angles, frequency ranges, layer arrangements, and layer thicknesses.

For a flat multilayer structure, the reflection coefficient with electrical and magnetic polarization values is defined as follows [4]:

$$RC^{TM/TE} = \frac{Z_i^{TM/TE} - Z_0^{TM/TE}}{Z_i^{TM/TE} + Z_0^{TM/TE}} \quad (1)$$

* Corresponding author.
E-mail address: Malekfar@modares.ac.ir (R. Malekfar).

http://dx.doi.org/10.1016/j.jmgm.2016.11.015
1093-3263/

$$RC_{dB}^{\frac{TM}{TE}} = 20log_{10}\frac{Z_i^{\frac{TM}{TE}} - Z_0^{\frac{TM}{TE}}}{Z_i^{\frac{TM}{TE}} + Z_0^{\frac{TM}{TE}}} \quad (2)$$

$$Z_0^{TM/TE} \cong 377\Omega \quad (3)$$

where $Z_0^{TM/TE}$ and $Z_i^{TM/TE}$ are free space impedance and ith layer impedance, respectively. The ith layer impedance ($Z_i^{TM/TE}$) is defined as follows:

$$Z_i^{TM/TE} = \eta_x^{TM/TE}\frac{Z_{ix-1}^{TM/TE}cos(k_x t_x) + j\eta_x^{TM/TE}sin(k_x t_x)}{\eta_x^{TM/TE}cos(k_x t_x) + jZ_{ix-1}^{TM/TE}sin(k_x t_x)} \quad (4)$$

where $\eta_x^{TM/TE}$ is intrinsic impedance, k_x is wavenumber, and t_x is thickness of the xth layer. On the other hand, complex permittivity and permeability for materials and the relationship with wavenumber, intrinsic impedance for two types of polarization, and incident angle of the xth layer are defined as follows:

$$\varepsilon_{rx} = \varepsilon_{rx}^{'} - j\varepsilon_{rx}^{''} \quad (5)$$

$$\mu_{rx} = \mu_{rx}^{'} - j\mu_{rx}^{''} \quad (6)$$

$$k_x^2 = (2\pi f)^2\varepsilon_0\mu_0\left(\varepsilon_{rx}^{'} - j\varepsilon_{rx}^{''}\right)\left(\mu_{rx}^{'} - j\mu_{rx}^{''}\right) \quad (7)$$

$$\eta_x^{TM} = \sqrt{\frac{\mu_0}{\varepsilon_0}}\sqrt{\frac{\mu_{rx}^{'} - j\mu_{rx}^{''}}{\varepsilon_{rx}^{'} - j\varepsilon_{rx}^{''}}}cos\theta_x \quad (8)$$

$$\eta_x^{TE} = \sqrt{\frac{\mu_0}{\varepsilon_0}}\sqrt{\frac{\mu_{rx}^{'} - j\mu_{rx}^{''}}{\varepsilon_{rx}^{'} - j\varepsilon_{rx}^{''}}}\frac{1}{cos\theta_x} \quad (9)$$

$$\theta_x = arc\sin\left(\frac{\sqrt{\varepsilon_{rx+1}}}{\sqrt{\varepsilon_{rx}}}\sin\theta_{x+1}\right) \quad (10)$$

Nanomaterials are suitable choice as multilayer absorbers. In the following, the optimization process for the number of layers, layer thickness, layer priorities, and the compounds of each layer is analyzed by the ISO algorithm [4].

2. Related work

The main issue in designing a planar microwave absorber is minimization of the reflection coefficient value of the incident wave on a multilayer structure in specific frequency and angle ranges. The reflection coefficient depends on layer thickness, electrical and magnetic properties of each layer. Minimization of the reflection coefficient is a multi-dimensional optimization problem and various studies can be done in this respect. Synthesis and composition can be controlled by dielectric coefficient, conductivity, thickness of the layer, and optimization in the number of layers by designing a model of multilayer absorber.

Many evolutionary algorithms have been used in designing the optimal absorbers. Particle Swarm Optimization (PSO) algorithm is proposed for optimization of problems like designing optimal absorbers. This algorithm is inspired from bird flocking scenario. The PSO algorithm cannot simultaneously deal with both continuous and discrete spaces and also cannot efficiently trade-off between exploration and exploitation abilities [5]. For these reasons, a new swarm-based algorithm is suggested in this paper; called ISO.

2.1. Proposed method

This section consists of three sub-sections. The first sub-section explains the PSO. In sub-section b, the ISO is explained, and sub-section c shows how to solve the MANM problem with the ISO.

One of the advantages of the ISO is the ability to simultaneously deal with the contentious and discrete dimensions; this ability is explained in sub-section b, [6].

2.1.1. Particle swarm optimization (PSO)

The behavior of bird flocking is simulated with PSO. Suppose there is only one piece of food in the area and a group of birds are randomly searching food in this area. For each iteration, all the birds know how far the food is, but certainly they do not know where the food is. The best strategy to find the food is to follow the bird that is the most nearest to the food.

The PSO algorithm is inspired from the bird flocking scenario and is used to solve the optimization problems. In PSO, each single solution is called "*particle*". All particles have fitness values that show the quality of particles; and have velocities, which direct the migration of the particles. The particles migrate through the problem space by following the current high quality particles [7].

PSO is initialized with a population of random individuals (particles) and then searches the search space by producing the generations. In each generation, each particle is updated by ascribing it to two "best" locations. The first one is the best location in terms of the fitness that the particle has found. This location is called p_{best}. The other "best" location that is tracked by the PSO is the best location obtained by any particle in the population. This best location is a global best and called g_{best}.

With the following Eqs. (11) and (12), the particle updates its location and velocity.

$$x_m^k(t+1) = x_m^k(t) + (t+1)v_m^k\Delta t \quad (11)$$

$$v_m^k(t+1) = W - inertia(t)v_m^k(t) + C_1(t).r_1(t).[P_{(best,m)}^k(t) - x_m^k(t)] + C_2(t).r_2(t).[G_{(best,m)}^{(t)} - x_m^k(t)] \quad (12)$$

x_m^k is the position value of the mth dimension in the kth particle, v_m^k is the velocity value of the mth dimension in the kth particle, *W-inertia* is inertia weight between [0–1]; C_1, C_2 are learning factors that are usually equal to 2; r_1, r_2 are random numbers between [0–1], and t is the time factor [8].

2.1.2. Imitation based optimization (ISO)

One of the most important problems in the optimization is the ability to deal with both exploration and exploitation. The exploration and exploitation abilities of an optimization algorithm cause the algorithm to adequately search the surface and the depth of the search space, respectively. Having both of them is difficult as the rise in exploration reduces the exploitation ability of the algorithm and vice versa. Most algorithms do not have high ability in both exploration and exploitation on the search space; but the ISO has the capability to trade-off between the exploration and exploitation with input parameters. In fact, the user can specify the importance of each ability. Another problem in optimization tasks is the ability to deal with both continuous and discrete spaces. The ISO simultaneously has this ability. In the ISO, instead of the 'particle' term, the 'individual' term is used. The ISO in the continuous space is similar to the PSO with some innovation but it has a new approach to deal with discrete spaces. The individuals in the ISO move toward better positions by imitating each other. This imitation is done in both continuous and discrete spaces. The pseudo code of the ISO procedure is as follows:

Pseudocode of the ISO procedure :

For each individual in the population

Initialize individuals with > random way

END

Do

For each individual in population

Calculate fitness value by Eq. (15)

If the current individual is better than the previous pBest in history

set current location of the individual as a new pBest

End

determine best individuals whitin current population as a new gBest

For each individual

Calculate individual velocity according to Eq. (13)

Update individual position according to Eq. (14)

End

While maximum iterations are not attained

equation(13) :

$if rand() < P_{rand} then$

$$v_m^k(t+1) = rand\left(\max_{velocity}, -\max_{velocity}\right)$$

else

$v_m^k(t+1)$ *is determined by Eq.* 12

equation(14) :

if the dimension is contenious then

$x_m^k(t+1)$ *is determined by Eq.* 11

else

$x_m^k(t+1) = x1$ *or* $x2$ *or* $x3$ *or* $x4$

equation(15) :

$$Fitness\ of\ individual = \sum_{freq=f_{min}}^{freq=f_{max}} \left(\sum_{\theta=\theta min}^{\theta=\theta max} RC_{TM}\left(freq, \theta\right) + RC_{TE}\left(freq, \theta\right)\right.$$

The fitness of the individual is equal to the sum of RLTMs and RLTEs values in the predefined range of frequencies and angles, which is shown by equation 5.

Where P_{rand} is the random velocity rate, $\max_{velocity}$ is the maximum velocity that is an input parameter, x_1 is the current position, x_2 is the new discrete random number, x_3 is the individual position in p_{best}, and x_4 is an individual position in the population that is selected by tournament way. Number of the tournaments is determined by *num of Tournament* (is an input parameter). In fact, the *num of Tournament* individuals is selected randomly and so the best value in terms of fitness is selected tox_4. Each of the x_1, x_2, x_3 and x_4 have a rate (w_1, w_2, w_3 and w_4 that are input parameters) and sum of them is equal to 1.

The P_{rand}, , w_2, , $r_1$andr_2 parameters are the exploration parameters and by increasing their values, exploration of the ISO can be maximized and vice versa. The *W-inertia,* w_3, w_4,c_1, andc_2 parameters are the exploitation parameters by increasing their values, the exploitation of the ISO can be maximized and vice versa. Also, by using equation 14, the algorithm is able to deal with discrete spaces.

2.1.3. MANM modeling with ISO

In order to model the MANM with ISO, a general view is suggested in this paper that is illustrated in Table 1 and shows individuals of the population in the *i*th generation. The rows show individuals that each has a current position and L_{best} position (the best position that the individual has already seen). The columns show the layer characteristics. Each layer has two dimensions: the material name and the material thickness. The number of layers for each individual (absorber structures) is determined by m and the number of individuals is determined by k.

The ISO produces *max-generation* (another input parameter), and in the process of the production tries to improve the fitness of the individuals according to the ISO policies. g_{best} is initialized with the best individual in the population and so it is used by equation 13 in each generation.

2.2. Experimental results

In this research, we investigate the reflection loss of 109 different structures presented in appendix. By having electrical permittivity and magnetic permeability coefficients of different compounds such as polymer composites, ferrites, hexaferrites, carbon materials, carbonyl-iron, it is possible to design an optimized tool for the best layer wave absorber. A selection of layer priority, layer arrangement, layer thickness, frequency range, and incident and polarization angles can be considered in the tool. The electrical permittivity and magnetic permeability coefficients used in this investigation are gathered from different sources [4,8–28].

The proposed tool includes four main menus. In the left panel of Fig. 1, the number of required layers, the number of used material, selection of minimum or maximum of permittivity and permeability values, frequency range, incident angle range, and layer thickness range are located. In the right panel of Fig. 1, there are parameters of the ISO algorithm.

Table 1
Individual population in the ith generation. The rows show a current and best position and the columns present the layer characterization.

		Layer 1	Layer 1	Layer 2	Layer 2	...	...	Layer m	Layer m
Ind. 1	Position	S_1	t_1	S_2	t_2	...	...	S_m	t_m
	L_{best}	LS_1	Lt_1	LS_2	Lt_2	...	...	LS_m	Lt_m
Ind. 2	Position	S_1	t_1	S_2	t_2	...	...	S_m	t_m
	L_{best}	LS_1	Lt_1	LS_2	Lt_2	...	...	LS_m	Lt_m
Ind. K	Position	S_1	t_1	S_2	t_2	...	...	S_m	t_m
	L_{best}	LS_1	Lt_1	LS_2	Lt_2	...	...	LS_m	Lt_m

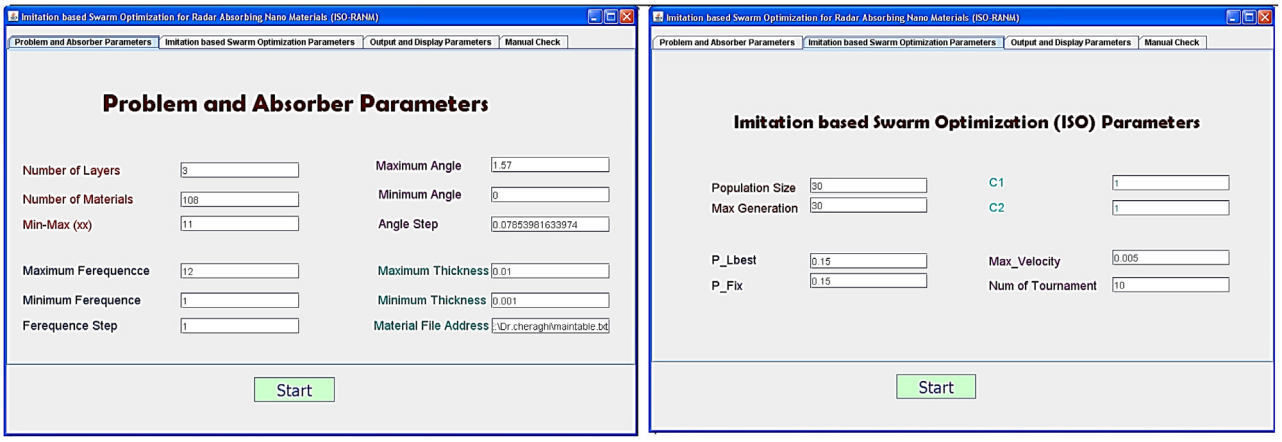

Fig. 1. Two main menus of the proposed tools of the algorithm. (left) Problem and absorber parameters; (right) Imitation based swarm optimization (ISO) parameters.

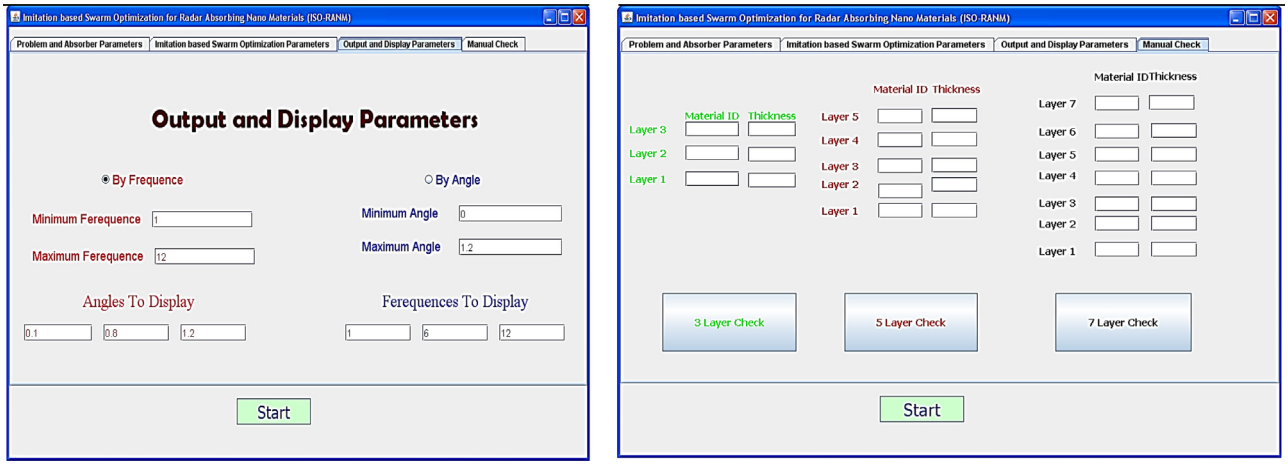

Fig. 2. Two main menus of the proposed tools of the algorithm. (left) Problem and absorber parameters; (left) Output and display parameters; (right) Material ID and thickness for 3, 5 and 7 layers.

Table 2
The algorithm output for three layer structure designed with the ISO.

Layer Type	ID	Material Type	t (mm)
Layer 2	ID = 74	Cu-NZF	t = 2.010041838195007
Layer 1	ID = 85	CIP/GRP composites	t = 1.0628852938473057
Layer 0	ID = 81	$BaTiO_3$/PANI%2	t = 2.86686151100

Table 3
The algorithm output for five layer structure designed with the ISO.

Layer Type	ID	Material Type	t (mm)
Layer 4	ID = 35	Air	t = 1.0
Layer 3	ID = 103	RAM + 40% carbonyl-iron	t = 1.0
Layer 2	ID = 1	F50% + PU100%	t = 1.0
Layer 1	ID = 14	PU + SWCNT15%	t = 1.0
Layer 0	ID = 23	PVC + $La(NO_3)$ 30.6% + ACNT 0.8%	t = 1.0

In the left panel of Fig. 1, the output and result parameters such as the frequency range and angle range are considered. After completion of the optimization, the user can manually change the output structure and can try new different forms of structures. This ability is shown in the right panel of Fig. 2. This information includes the number of layers, type of materials, and the proposed thickness.

In this step, various outputs can be observed by various sets of composition. A three-layer structure that is designed with the ISO is illustrated in Table 2 with approximate thickness of 6 mm.

The reflection coefficient is measured in 1–12 GHz frequency range and 0–90° angle range for TM and TE polarization. As shown in Fig. 3 (left), the maximum reflection loss is about −34 (dB) at the frequency of 8.5 GHz and for 30° angle for the TE wave. In Fig. 3 (right), the maximum reflection loss is −20 (dB) at frequency of 7 GHz and 0° angle for the TM wave.

As shown in Fig. 4 (left), the maximum reflection loss is about −34 (dB) at 12 GHz frequency and 53° angle and for the TE wave. In Fig. 4 (right), the maximum reflection loss is −16.5 (dB) at 6 GHz frequency and 10° angle and for the TM wave.

In this step, various outputs can be achieved using various sets of composition. A five-layer structure designed with the ISO is illustrated in Table 3. The structure is designed with an approximate thickness of 5 mm.

The reflection coefficient value is measured in 1–12 GHz frequency range and 0–90° angle range for TM and TE polarizations. As shown in Fig. 5 (left), the maximum reflection loss is about −32 (dB) at frequency of 8.5 GHz and 0° angle for the TE wave. In Fig. 5 (right), the maximum reflection loss is −41 (dB) at frequency of 8.5 GHz and 30° angle for the TM wave.

As shown in Fig. 6 (left), the maximum reflection loss is about −14 (dB) in the frequency of 6 GHz and 10° angle for the TE wave. In Fig. 6 (right), the maximum reflection loss is −17 (dB) in the frequency of 6 GHz and 85° angle for the TM wave.

In this step, the results for a seven-layer structure, Table 4, designed with an approximate thickness of 7 mm using the ISO-MANM tool are provided.

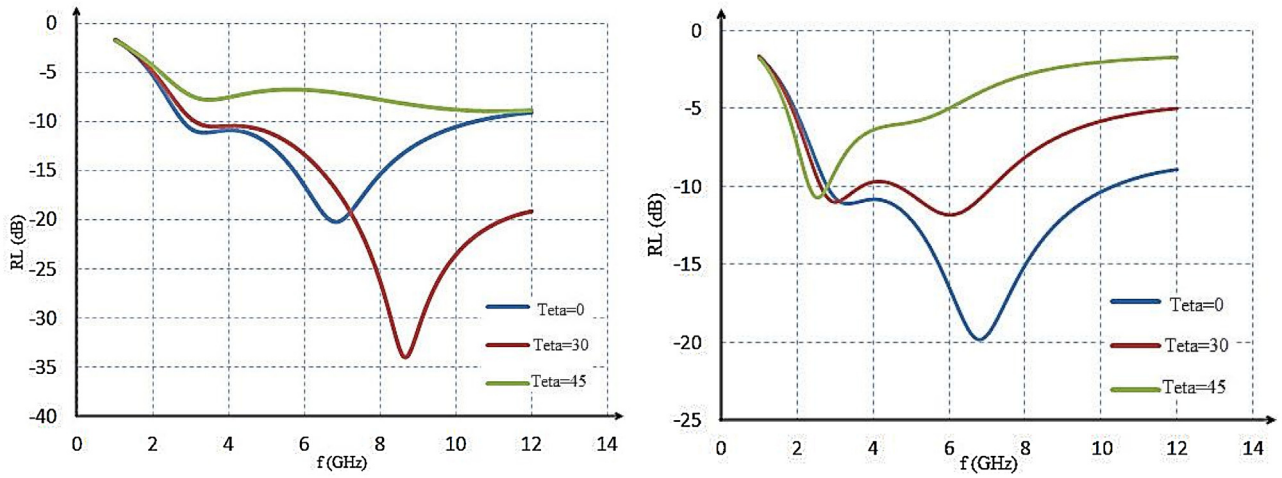

Fig. 3. The reflection coefficient values in the 1–12 GHz frequency range and for angles of 0, 30, and 45°; TE polarization (left) and TM polarization (right); for three layer structure.

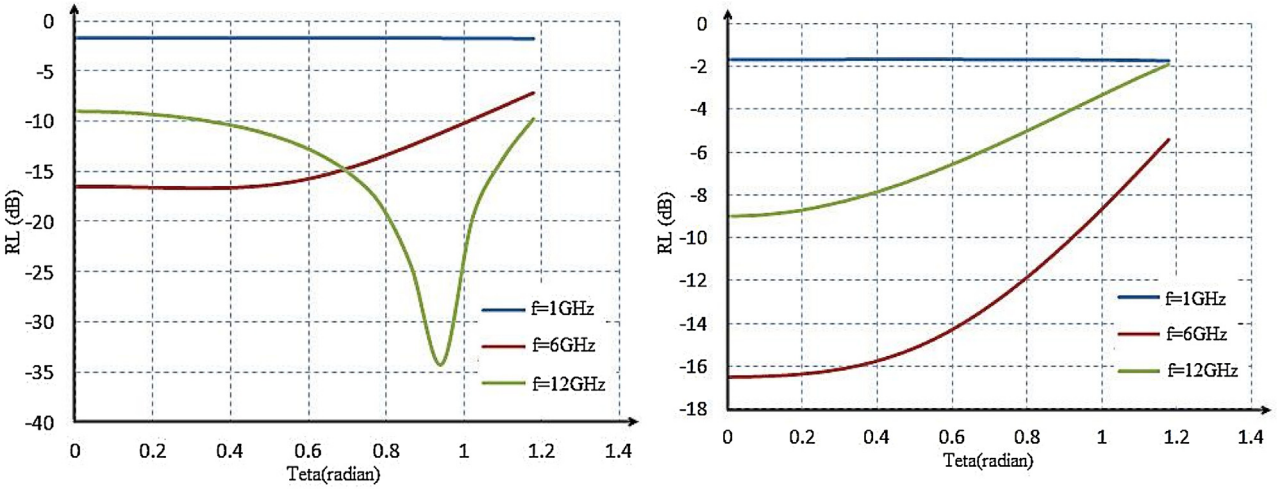

Fig. 4. The reflection coefficient values in the 0–90° angle range and 1, 6, and 12 GHz frequencies; for TE polarization (left) and TM polarization (right); for three layer structure.

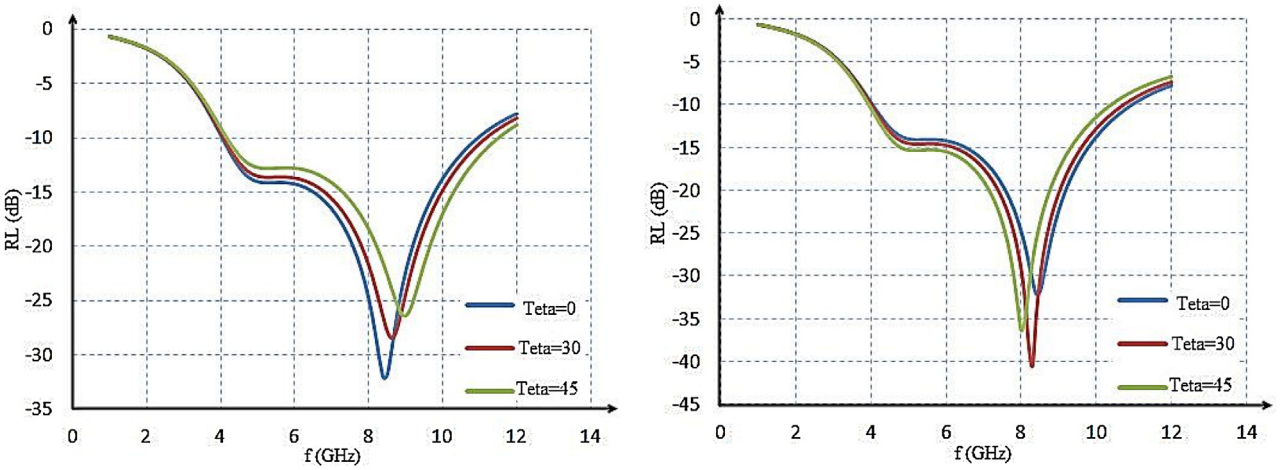

Fig. 5. The reflection coefficient values in the 1–12 GHz frequency range and 0, 30, and 45° angles; TE polarization (left) and TM polarization (right); for five layer structure.

The reflection coefficient value is measured in 1–12 GHz frequency range and 0–90° angle range for TM and TE polarization. As shown in Fig. 7 (left), the maximum reflection loss is about −32 (dB) in the frequency of 9 GHz and 0° angle for the TE wave. In Fig. 7 (right), the maximum reflection loss is −32 (dB) in the frequency of 9 GHz and 0° angle for the TM wave.

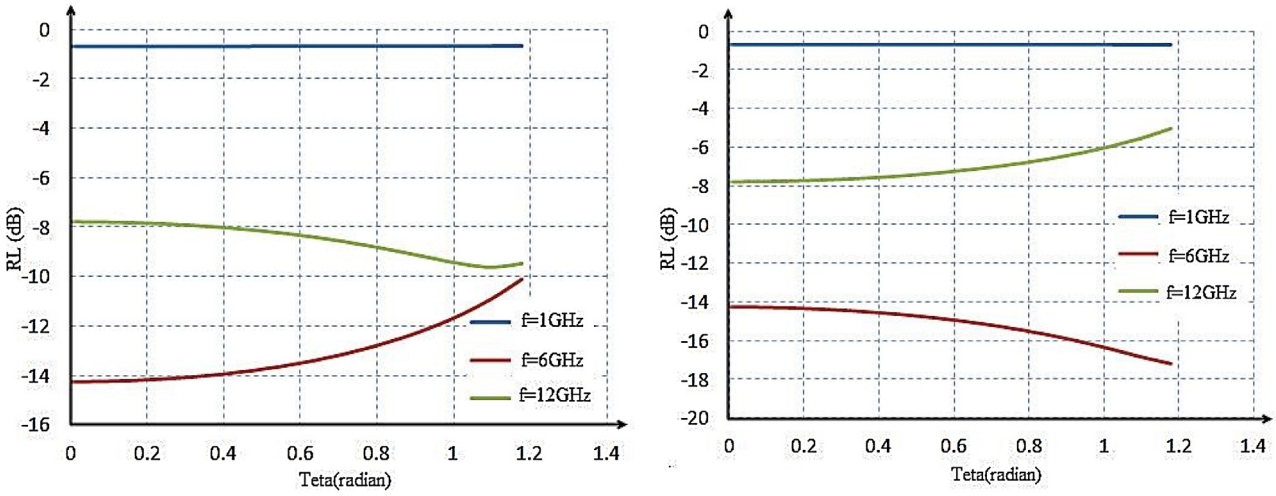

Fig. 6. The reflection coefficient values in the 0–90° angle range and 1, 6, and 12 GHz frequencies; for TE polarization (left) and TM polarization (right); for five layer structure.

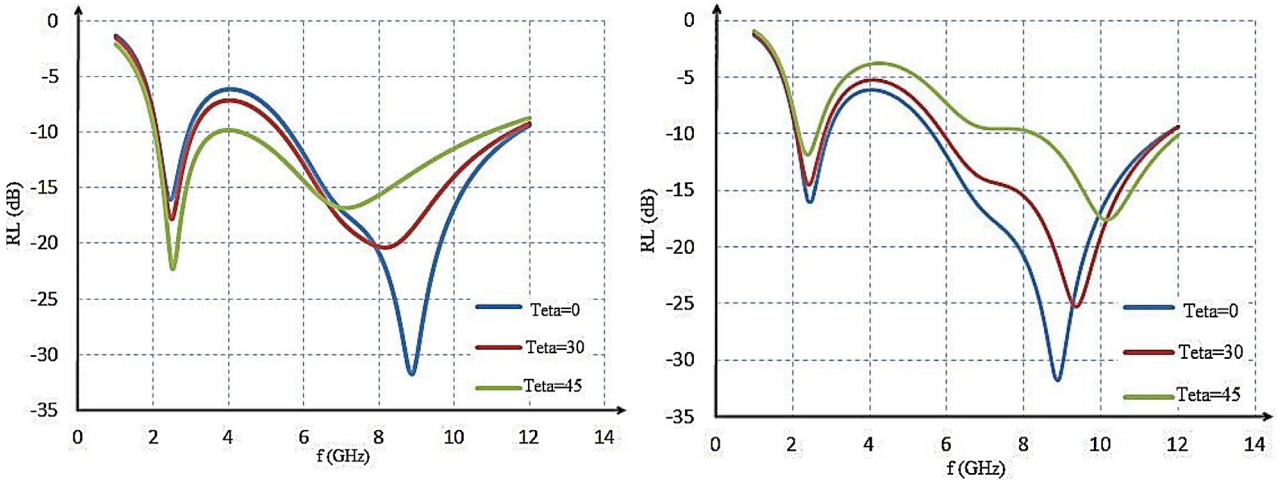

Fig. 7. The reflection coefficient values in the 1–12 GHz frequency range and angles of 0, 30, and 45°; TE polarization (left) and TM polarization (right); for seven layer structure.

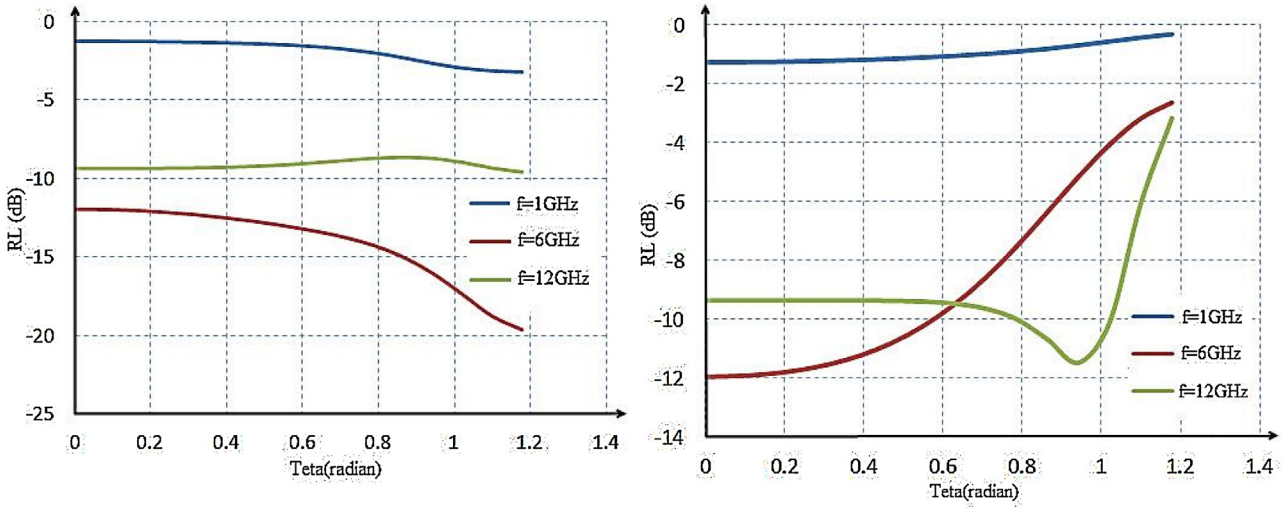

Fig. 8. The reflection coefficient values in the 0–90° angle range and 1, 6, and 12 GHz frequencies; for TE polarization (left) and TM polarization (right); for seven layer structure.

Table 4
The algorithm output for seven layer structure designed with the ISO.

Layer Type	ID	Material Type	t (mm)
Layer 6	ID = 1	$Ba_{(1-x)}LaxFe_{12}O_{19(x=0.05)}$	t = 1.0
Layer 5	ID = 108	E.R + MWCNT 7%	t = 1.0
Layer 4	ID = 89	Carbonyl-iron/ $Fe_{91}Si_9$ composites (9:1)	t = 1.0
Layer 3	ID = 1	F 50% + PU 100%	t = 1.0
Layer 2	ID = 58	E.R + CNF 3%	t = 1.0
Layer 1	ID = 89	Carbonyl-iron/ Fe91Si9 composites(9:1)	t = 1.0
Layer 0	ID = 1	F 50% + PU 100%	t = 1.0

As shown in Fig. 8 (left), the maximum reflection loss is about −20 (dB) in the frequency of 6 GHz and for 90° angle for the TE wave. In Fig. 8 (right), the maximum reflection loss is −12 (dB) in the frequency of 6 GHz and 10° angle for the TM wave.

3. Conclusion

In designing multilayer microwave absorber area, minimization of the reflection coefficient and the intensity of the incident wave for a structure in a specific range of angles and frequencies is important. The reflection loss depends on thickness, electrical and magnetic properties for each layer, layers priority, and total thickness of the multilayer. The process of minimization of the reflection loss needs a strong optimization algorithm with high quality trade-off ability between exploration and exploitation abilities. Also, the optimization algorithm must have the ability to deal with two spaces (discrete and continuous). Synthesis and composition can be controlled in dielectric coefficient, conductivity, thickness of the layer, and optimization in the number of layers by designing a model of multilayer absorber.

The ISO algorithm was designed to satisfy the above requirements. By implementing the ISO algorithm, we achieved our objectives including reflection losses with different polarizations, number of layers, the desired thickness, different incident angles, and priority placement of layers. Reference library of the composites is achieved by studying performance of different materials to reduce reflection in microwave range and making use of the results of the studies performed on composites, carbonyl iron, different CNTs, and ferrites. These materials helped our tool with different ranges of permittivity and permeability coefficients. Equations of reflection loss are written for the tool with TE and TM polarizations, incident angles, different permittivity and permeability coefficients, radiation frequencies, and thickness values. In the current paper, a new swarm-based algorithm was suggested to solve the MANM problem. The individuals in the ISO imitate each other and move to better locations. The ISO has a high ability to trade-off between the exploration and exploitation by setting the input parameters. It can also simultaneously deal with contentious and discrete spaces. The results obtained demonstrated that our proposed method has high quality outcomes and can be used in various applications.

Appendix A. 109 different structures consisting of polymer composites, ferrites, hexaferrites, carbon materials, carbonyl-iron, etc. with their related electrical permittivity and magnetic permeability coefficients which used in this research and as the input values for the proposed optimized tool for investigating the best layer wave absorber (Refer to the related references for more details).

Num.	Material Type	ε'_1	ε'_2	ε''_1	ε''_2	μ'_1	μ'_2	μ''_1	μ''_2	Reference
1	F 50% + PU 100%	5.4	5.4	0.15	2.2	1.22	1.08	0.05	0.08	[9]
2	F 60% + PU 100%	7.8	7.8	0.3	0.5	1.2	1.05	0.06	0.1	[9]
3	F 70% + PU 100%	9.5	9.5	0.4	0.5	1.29	1	0.08	0.11	[9]
4	F 80% + PU 100%	14.5	14.5	0.9	1.3	1.27	1.14	0.1	0.13	[9]
5	E.R + MWCNT 4.7%	6	5	1	2	1	1	0	0	[10]
6	E.R + MWCNT 11.4%	22	14	7	4	1	1	0	0	[10]
7	E.R + MWCNT 23.1%	160	5	200	10	1	1	0	0	[10]
8	E.R + MWCNT 25.9%	200	20	200	20	1	1	0	0	[10]
9	E.R + Fe + MWCNT 16.7%	35	24	90	42	1	1	0	0	[10]
10	PS + Fe + MWCNT 20%	30	25	0.9	0.6	1	1	0	0	[10]
11	PU + SWCNT 20%	37	30	26	24	1	1	0	0	[10]
12	P.U + SWCNT 5%	6	6	2	2	1	1	0	0	[11]
13	P.U + SWCNT 10%	18	19	10	12	1	1	0	0	[11]
14	P.U + SWCNT 15%	31	32	17	32	1	1	0	0	[11]
15	P.U + SWCNT 20%	32	38	23	27	1	1	0	0	[11]
16	E.R + CNT (20%)	20	31	20	50	0.01	0.01	0.01	0.01	[12]
17	E.R + CNT 10% + Fe 10%	20	34	47	58	0.8	1	0.03	0.03	[12]
18	E.R + CNF 10%+ Fe 10%	26	35	30	70	0.8	1.1	0.03	0.03	[12]
19	E.R + CNT 10% + Fe 10%	27	32	48	55	1.7	2.1	1.4	1.7	[12]
20	E.R + CNF 10% + Fe 10%	28	33	45	92	1.9	2.3	1.4	1.9	[12]
21	PVC + MWCNT 0.8%	8	8.3	1.2	1.4	1.1	1.2	1-0.1	0.1	[13]
22	PVC + ACNT 0.8%	5.5	5.6	0.8	0.9	1.2	1.3	0.11	0.14	[13]
23	PVC + La(NO3)3 0.6% + ACNT 0.8%	5.8	7.5	1.8	3.5	1	1.6	0.17	0.3	[13]
24	Pure E.R	2.60	2.80	0.05	0.10	1.30	1.20	0.10	-0.05	[14]
25	E.R + MWCNT 1%	3.40	3.60	0.20	0.25	1.40	1.30	0.10	0.10	[14]
26	E.R + MWCNT 2%	3.50	3.50	0.18	0.22	1.40	1.40	0.10	0.10	[14]
27	E.R + MWCNT 3%	3.80	3.90	0.28	0.31	1.30	1.30	0.10	0.10	[14]
28	E.R + MWCNT 4%	5.20	5.30	0.40	0.60	1.40	1.30	0.10	0.10	[14]
29	E.R + MWCNT 5%	5.40	5.60	0.50	0.85	1.40	1.30	0.10	0.10	[14]
30	E.R + MWCNT 6%	6.60	6.80	0.60	1.20	1.40	1.20	0.10	0.10	[14]
31	E.R + MWCNT 7%	6.70	6.90	0.50	1.20	1.40	1.20	0.10	0.10	[14]
32	E.R + MWCNT 8%	7.40	7.50	0.60	1.50	1.40	1.30	0.10	0.10	[14]
33	E.R + MWCNT 9%	7.80	8.00	0.60	1.40	1.10	1.00	0.10	0.10	[14]
34	E.R + MWCNT 10%	7.90	8.30	0.80	1.90	1.40	1.10	0.10	0.10	[14]
35	Air	1	1	0	0	1	1	0	0	[8]
36	Teflon	2	2	0	0	1	1	0	0	[8]
37	E.R	2.8	2.8	0.1	0.1	1	1	0	0	[8]
38	E.R + MWCNT 0.5%	5.5	4	1.2	1.4	1	1	0	0	[8]

39	E.R + MWCNT 1%	7	5.7	1.5	1.8	1	1	0	0	[8]
40	E.R + MWCNT 1.5%	10	7	2.7	3.2	1	1	0	0	[8]
41	E.R	4	4	1	1	1	1	0	0	[4]
42	E.R + MWCNT 0.5%	4	7	2	3	1	1	0	0	[4]
43	E.R + MWCNT 1%	7	8	3	4	1	1	0	0	[4]
44	E.R + MWCNT 2%	9	12	4	7	1	1	0	0	[4]
45	E.R + MWCNT 2.5%	14	15	10	12	1	1	0	0	[4]
46	E.R + MWCNT 3%	17	18	14	15	1	1	0	0	[4]
47	E.R + MWCNT 4%	29	32	25	28	1	1	0	0	[4]
48	E.R + SWCNT 1%	3.8	4	0.5	0.6	1	1	0	0	[15]
49	E.R + SWCNT 3%	5.7	5.8	1.4	1.6	1	1	0	0	[15]
50	E.R + SWCNT 5%	7.5	7.8	2.4	2.8	1	1	0	0	[15]
51	E.R + Graphite 1%	3.1	3.2	0.2	0.2	1	1	0	0	[15]
52	E.R + Graphite 3%	3.5	3.8	0.1	0.1	1	1	0	0	[15]
53	E.R + Graphite 5%	3.5	3.8	0.1	0.1	1	1	0	0	[15]
54	E.R + Fullerene 1%	3.2	3.4	0.2	0.3	1	1	0	0	[15]
55	E.R + Fullerene 3%	3.5	3.8	0.3	0.3	1	1	0	0	[15]
56	E.R + Fullerene 5%	4	4.1	0.1	0.2	1	1	0	0	[15]
57	E.R + CNF 1%	7.1	8	2.7	2.8	1	1	0	0	[15]
58	E.R + CNF 3%	12.8	15	6	6.2	1	1	0	0	[15]
59	E.R + CNF 5%	15	17	7	7.3	1	1	0	0	[15]
60	Fe_3O_4	4.9	5.5	1.3	1.6	0.8	1.1	0.1	0.2	[16]
61	$BaFe_{12}O_{19}$	1.42	1.50	0	0	1.04	1.14	0	0	[16]
62	$SrFe_{12}O_{19}$	1.22	1.5	0	0	1.05	1.12	0	0	[16]
63	wax comp. (wax-30% Ni/MWCNT (δ=3))	6	8	1	4	0.96	1.07	−0.01	0.11	[17]
64	wax comp.(wax-30% Ni/MWCNT (δ=7.5))	7.4	12.4	1.25	4	0.94	1.12	−0.01	0.23	[17]
65	wax comp. (wax-30% Ni/MWCNT (δ=15))	18.5	36.25	11.25	62.5	0.85	1.42	0.01	0.36	[17]
66	$BaFe_{12}O_{19}$/a-Fe_2O_3 (Fe/BaM 1:8)	4.25	5.9	0.1	1.1	0.92	1.15	0.06	0.15	[18]
67	$BaFe_{12}O_{19}$/a-Fe_2O_3 (Fe/BaM 1:6)	4.9	6.4	0.55	1.75	1	1.2	0.06	0.20	[18]
68	$BaFe_{12}O_{19}$/a-Fe_2O_3 (Fe/BaM 1:4)	4.6	6.15	0.35	1.2	0.97	1.2	0.08	0.185	[18]
69	$BaFe_{12}O_{19}$/a-Fe_2O_3 (Fe/BaM 1:2)	3.9	4.55	0	0.35	0.8	1.4	0.02	0.325	[18]
70	Activated Carbon	3	3	0	0	0.3	0.98	−0.24	0	[10]
71	PGCFs (700 °C)	10	40	8	44	0.92	0.98	−0.07	−0.04	[10]
72	PGCFs (800 °C)	19	90	22	76	0.89	1.06	0	0.15	[10]
73	PGCFs (900 °C)	19	119	59	135	0.52	0.76	0.02	0.25	[10]
74	Cu-NZF	3.73	3.85	0.063	0.16	0.93	1.11	0.025	0.19	[19]
75	Cu-NZF/PZT (3 : 1)	3.89	3.95	0.2	0.25	0.97	1.15	0.015	0.17	[19]
76	Cu-NZF/PZT (1 : 1)	4.02	4.1	0.23	0.26	1	1.15	0.01	0.06	[19]
77	Cu-NZF/PZT (1 : 3)	4.15	4.2	0.16	0.21	1.02	1.16	0.01	0.075	[19]
78	PZT	4.4	4.53	0.14	0.17	1	1	0	0	[19]
79	$BaTiO_3$/ polyaniline (PANI%0)	20	30	15	30	0.75	1.75	0.1	1.25	[20]
80	$BaTiO_3$/ polyaniline (PANI%0.5)	8	48	10	19	0.9	1.5	0	0.6	[20]
81	$BaTiO_3$/ polyaniline(PANI%2)	10	28	5	20	0.75	1.6	0	0.75	[20]
82	$BaTiO_3$/ polyaniline (PANI%4)	5	183	0	158	0.6	2.4	0	2.2	[20]
83	$BaTiO_3$/ polyaniline (PANI%6)	20	50	5	50	1	2.5	0	1.8	[20]
84	$BaTiO_3$/ polyaniline (PANI%8)	10	38	1	12	0	6	0	2.2	[20]
85	CIP/GRP composites	6.2	11.2	0	3.9	1.7	3.1	0.55	1.25	[21]
86	TiO_2 powder (M40)	13	13.75	1	1.25	1	1.05	0	0.03	[22]
87	M41	32	34	2.6	5	1	1	−0.01	0.01	[22]
88	M42	16.25	17.5	1.25	3.75	1	1	−0.01	0.02	[22]
89	Carbonyl-iron/$Fe_{91}Si_9$ composites (9:1)	27.5	35	6	13.5	1.4	2.5	0.6	0.81	[23]
90	Carbonyl-iron/$Fe_{91}Si_9$ composites (2.3:1)	22	24.5	2.4	4.8	1.35	2.25	0.54	0.72	[23]
91	Carbonyl-iron/$Fe_{91}Si_9$ composites (1:1)	14.5	15	1.25	2	1.3	2.2	0.42	0.6	[23]
92	carbonyl-iron powders (CIP)	29.5	44.5	10	24.5	1.6	2.85	0.64	1.01	[23]
93	$Fe_{91}Si_9$ powders (FSP)	10	10	0	0	0.9	1.65	0.24	0.32	[23]
94	M	5.1	5.3	0.1	0.2	1.035	1.056	0.027	0.06	[24]
95	MC	7.65	8.5	1.45	1.8	1.041	1.071	0.015	0.042	[24]
96	MWCNT (30%) + TPU	14.9	15.9	2.75	3.5	1	1	0	0	[25]
97	TiO_2 (30%) + TPU	3.5	4	−0.25	0	1	1	0	0	[25]
98	TiO_2 coated MWCNT (30%) + TPU	5	5	0.8	1.1	1	1	0	0	[25]
99	TiO_2 coated MWCNT (15%) + Fe_3O_4 (15%)	6.5	7	1.25	1.5	1	1.2	-0.05	0.07	[25]
100	RAM	2.5	3.8	−0.1	−0.1	1	1.2	0	0	[26]
101	RAM + 20% carbonyl iron	3	7.5	0.3	0.3	1	2	0.4	0.55	[26]
102	RAM + 30% carbonyl-iron	3.8	9	0.4	0.5	1	2.4	0.6	0.8	[26]
103	RAM + 40% carbonyl-iron	4	12	1	1.08	1	3.2	0.9	1.35	[26]
104	RAM + 45% carbonyl-iron	5.7	14	1.35	1.45	1	3.5	1	1.7	[26]
105	Graphene	18	20	7.5	9.5	0.88	1.1	-0.45	0.082	[27]
106	MWCNT	14.9	15.9	2.8	4	0.89	1.1	-0.05	0.025	[27]
107	$Ba_{(1-x)}La_xFe_{12}O_{19}$ (x = 0)	3.5	3.66	0.01	0.16	1	1.1	0.01	0.05	[28]
108	$Ba_{(1-x)}La_xFe_{12}O_{19}$ (x = 0.05)	3.74	4.2	0.28	0.28	1.25	3.9	0.36	0.42	[28]
109	$Ba_{(1-x)}La_xFe_{12}O_{19}$ (x = 0.1)	3.65	3.8	0.01	0.12	0.8	1.1	0.01	0.08	[28]

References

[1] F. Qin, C. Brosseau, A review and analysis of microwave absorption in polymer composites filled with carbonaceous particles, J. Appl. Phys. 111 (2012), http://dx.doi.org/10.1063/1.3688435, 061301.

[2] F. Wen, F. Zhang, J. Xiang, W. Hu, S. Yuan, Z. Liu, Microwave absorption properties of multiwalled carbon nanotube/FeNi nanopowders as light-weight microwave absorbers, J. Magn. Magn. Mater. 343 (2013) 281–285, http://dx.doi.org/10.1016/j.jmmm.2013.05.010.

[3] Z. Liu, G. Bai, Y. Huang, F. Li, Y. Ma, T. Guo, et al., Microwave absorption of single-walled carbon nanotubes/soluble cross-linked polyurethane composites, J. Phys. Chem. C (2007) 13696–13700.

[4] D. Micheli, C. Apollo, R. Pastore, R. Bueno Morles, S. Laurenzi, M. Marchetti, Nanostructured composite materials for electromagnetic interference shielding applications, Acta Astronaut. 69 (2011) 747–757, http://dx.doi.org/10.1016/j.actaastro.2011.06.004.

[5] H. Ri, H.U.V. Iru, U. Ehwzhhq, Diseño óptimo de absorbedores electromagnéticos multicapa para frecuencias en el rango de 0,85–5,4 GHz (2013) 33–37.

[6] M. Asi, N. Dib, Design of multilayer microwave broadband absorbers using central force optimization, Prog. Electromagn. Res. B 26 (2010) 101–113, http://dx.doi.org/10.2528/PIERB10090103.

[7] S. Chamaani, S.A. Mirtaheri, M. Teshnehlab, M.A. Shoorehdeli, V. Seydi, Optimization for electromagnetic absorber design, Technology 79 (2008) 353–366.

[8] D. Micheli, R. Pastore, G. Gradoni, V. Mariani Primiani, F. Moglie, M. Marchetti, Reduction of satellite electromagnetic scattering by carbon nanostructured multilayers, Acta Astronaut. 88 (2013) 61–73, http://dx.doi.org/10.1016/j.actaastro.2013.03.003.

[9] S.M. Abbas, R. Dixit, T.C. Goel, Complex permittivity, complex permeability and microwave absorption properties of ferrite–polymer composites, J. Magn. Magn. Mater. 309 (2007) 20–24, http://dx.doi.org/10.1016/j.jmmm.2006.06.006.

[10] Q. Liu, B. Cao, C. Feng, W. Zhang, S. Zhu, D. Zhang, High permittivity and microwave absorption of porous graphitic carbons encapsulating Fe nanoparticles, Compos. Sci. Technol. 72 (2012) 1632–1636, http://dx.doi.org/10.1016/j.compscitech.2012.06.022.

[11] Z. Liu, G. Bai, Y. Huang, Y. Ma, F. Du, F. Li, et al., Reflection and absorption contributions to the electromagnetic interference shielding of single-walled carbon nanotube/polyurethane composites, Carbon N. Y. 45 (2007) 821–827, http://dx.doi.org/10.1016/j.carbon.2006.11.020.

[12] R.C. Che, L.-M. Peng, X.F. Duan, Q. Chen, X.L. Liang, Microwave absorption enhancement and complex permittivity and permeability of Fe encapsulated within carbon nanotubes, Adv. Mater. 16 (2004) 401–405, http://dx.doi.org/10.1002/adma.200306460.

[13] T. Zhao, C. Hou, H. Zhang, R. Zhu, S. She, J. Wang, et al., Electromagnetic wave absorbing properties of amorphous carbon nanotubes, Sci. Rep. 4 (2014) 1–7, http://dx.doi.org/10.1038/srep05619.

[14] Z. Wang, G.-L. Zhao, Microwave absorption properties of carbon nanotubes-epoxy composites in a frequency range of 2–20 GHz, Open J. Compos. Mater. 03 (2013) 17–23, http://dx.doi.org/10.4236/ojcm.2013.32003.

[15] D. Micheli, C. Apollo, R. Pastore, M. Marchetti, X-Band microwave characterization of carbon-based nanocomposite material, absorption capability comparison and RAS design simulation, Compos. Sci. Technol. 70 (2010) 400–409, http://dx.doi.org/10.1016/j.compscitech.2009.11.015.

[16] A. Sharma, M.N. Afsar, Microwave complex permeability and permittivity of nanoferrites, J. Appl. Phys. 109 (2011), http://dx.doi.org/10.1063/1.3536659, 07A503.

[17] G. Tong, F. Liu, W. Wu, F. Du, J. Guan, Rambutan-like Ni/MWCNT heterostructures: easy synthesis, formation mechanism, and controlled static magnetic and microwave electromagnetic characteristics, J. Mater. Chem. A 2 (2014) 7373, http://dx.doi.org/10.1039/c4ta00117f.

[18] X.-C. Yang, R.-J. Liu, X.-Q. Shen, F.-Z. Song, M.-X. Jing, X.-F. Meng, Enhancement of microwave absorption of nanocomposite $BaFe_{12}O_{19}$/α-Fe microfibers, Chin. Phys. B 22 (2013), http://dx.doi.org/10.1088/1674-1056/22/5/058101, 058101.

[19] N. Zinc, F. Pb, Z. Ti, A. Mandal, D. Ghosh, A. Malas, et al., Synthesis and microwave absorbing properties of Cu-doped, J. Eng. (2013), 2013.

[20] L. Hongxia, Y. Qiaoling, G. Yun, Preparation and microwave adsorption properties of core–shell structured barium titanate/polyaniline composite, J. Magn. Magn. Mater. 332 (2013) 10–14, http://dx.doi.org/10.1016/j.jmmm.2012.11.010.

[21] Y. Tan, J. Tang, A. Deng, Q. Wu, T. Zhang, H. Li, Magnetic properties and microwave absorption properties of chlorosulfonated polyethylene matrices containing graphite and carbonyl-iron powder, J. Magn. Magn. Mater. 326 (2013) 41–44, http://dx.doi.org/10.1016/j.jmmm.2012.08.021.

[22] A. Kumar, V. Agarwala, D. Singh, Microwave absorbing behavior of metal dispersed TiO2 nanocomposites, Adv. Powder Technol. 25 (2014) 483–489, http://dx.doi.org/10.1016/j.apt.2013.07.006.

[23] J. Guo, Y. Duan, L. Liu, L. Chen, S. Liu, Electromagnetic and microwave absorption properties of carbonyl-iron/Fe91Si9 composites in gigahertz range, J. Electromagn. Anal. Appl. 03 (2011) 140–146, http://dx.doi.org/10.4236/jemaa.2011.35023.

[24] G.Z. Shen, G.S. Cheng, Y. Cao, Z. Xu, Preparation and microwave absorption of M type ferrite nanoparticle composites, Mater. Sci. 28 (2010) 327–334.

[25] P. Bhattacharya, Microwave absorption behaviour of MWCNT based nanocomposites in X-band region, Express Polym. Lett. 7 (2013) 212–223, http://dx.doi.org/10.3144/expresspolymlett.2013.20.

[26] Y. Feng, T. Qiu, X. Li, C. Shen, Microwave absorption properties of the carbonyl iron/EPDM radar absorbing materials, J. Wuhan Univ. Technol. Sci. Ed. 22 (2007) 266–270, http://dx.doi.org/10.1007/s11595-005-2266-9.

[27] C.K. Das, P. Bhattacharya, S.S. Kalra, Graphene and MWCNT: potential candidate for microwave absorbing materials, J. Mater. Sci. Res. 1 (2012) 126–132, http://dx.doi.org/10.5539/jmsr.v1n2p126.

[28] C.-J. Li, B. Wang, J.-N. Wang, Magnetic and microwave absorbing properties of electrospun Ba(1-x)LaxFe12O19 nanofibers, J. Magn. Magn. Mater. 324 (2012) 1305–1311, http://dx.doi.org/10.1016/j.jmmm.2011.11.016.